AGU PUBLICATIONS

JGR

Journal of Geophysical Research: Space Physics

RESEARCH ARTICLE

10.1002/2015JA022104

Key Points:
- Correlation between ULF waves and polar cap atmospheric dynamics
- Solar Wind variability influence on high-latitude atmosphere
- Relativistic electrons precipitation and cloud formation

Correspondence to:
M. Regi,
mauro.regi@aquila.infn.it

Citation:
Regi, M., M. De Lauretis, G. Redaelli, and P. Francia (2016), ULF geomagnetic and polar cap potential signatures in the temperature and zonal wind reanalysis data in Antarctica, *J. Geophys. Res. Space Physics*, *121*, doi:10.1002/2015JA022104.

Received 30 OCT 2015
Accepted 22 DEC 2015
Accepted article online 28 DEC 2015

ULF geomagnetic and polar cap potential signatures in the temperature and zonal wind reanalysis data in Antarctica

M. Regi[1], M. De Lauretis[1], G. Redaelli[2], and P. Francia[1]

[1]Department of Physical and Chemical Sciences, University of L'Aquila, L'Aquila, Italy, [2]CETEMPS/Department of Physical and Chemical Sciences, University of L'Aquila, L'Aquila, Italy

Abstract In the present study we investigated the possible coupling between geomagnetic activity and the low atmosphere dynamics in the polar cap. We compared daily values of the ERA-Interim temperature and zonal wind over Antarctica, with the daily geomagnetic ULF power, in the Pc5 (1–7 mHz), Pc1, and Pc2 (100 mHz–1 Hz) frequency ranges, at Terra Nova Bay (Antarctica, corrected geomagnetic latitude $\lambda \sim 80°$S) and with solar wind data during 2007, in correspondence to the last declining phase of the solar cycle 23. We found a high and statistically significant correspondence of temperature and zonal wind fluctuations in the stratosphere and troposphere with geomagnetic ULF power fluctuations at the ~27 day periodicity, with a substantial reduction at the tropopause height. A similar, clear relationship between the meteorological parameters and the polar cap potential difference was also observed. The results suggest that the changes in the atmospheric conductivity, due to energetic electrons precipitation driven by the ULF waves, as well as the high latitude potential variations, both associated to high geomagnetic activity, can affect the atmospheric dynamics.

1. Introduction

The near-Earth space is affected by complex phenomena due to the impact of the Sun's energy released via electromagnetic radiation (radiative source) and solar wind (SW). The radiative input is regarded as primary energy source, since its level is about million times greater than the SW [*Dudok de Wit and Watermann*, 2010; *Gray et al*., 2010]; however, significant variations in the SW energy, causing perturbed geomagnetic periods, can affect significantly the Earth's atmosphere. Geomagnetic activity driven signatures have been found in meteorological and climate records [e.g., *Lu et al*., 2008; *Seppälä et al*., 2009; *Lockwood et al*., 2010], but it is still not clear how the geomagnetic activity variations could influence the climate variables such as stratospheric and tropospheric temperatures [*Seppälä et al*., 2013].

A possible relationship between the SW and geomagnetic conditions and the Earth's atmosphere is probably due to the high-latitude energetic electron precipitation that produces, by ionization processes, effects characterized by different time delays in the atmospheric response. The longer-term response (on scales of several weeks) is usually attributed to odd nitrogen (NOx) production in the mesosphere and lower thermosphere. During the polar winter, NOx can live long enough to be transported, more effectively inside the polar vortex, to stratospheric ozone levels, where it chemically perturbs the ozone distribution, altering the radiative balance in that region of the atmosphere; this eventually leads to detectable changes in surface air temperatures through dynamical coupling, with the whole process occurring on time scales of several weeks [e.g., *Randall et al*., 2005, 2007; *Seppälä et al*., 2007, 2009, 2013, 2014; *Verronen et al*., 2011; *Andersson et al*., 2012; *Rozanov et al*., 2005; *Lu et al*., 2008; *Baumgaertner et al*., 2011; *Mironova et al*., 2015].

On the other hand, the shorter-time response (<1 day) is probably related to changes in the electric conductivity in the lower atmosphere by ionization and/or to changes of the polar cap electric potential induced by SW perturbations [*Mironova et al*., 2015]; the consequent modulation of the current density which flows from the upper boundary (being as low as 60 km) [*Tinsley*, 2008] through the troposphere to the ground in the global electric circuit (GEC) [*Tinsley and Zhou*, 2006; *Tinsley et al*., 2007; *Tinsley*, 2008; *Rycroft et al*., 2012; *Lam and Tinsley*, 2015] could influence cloud formation through the release of latent heat, which in turn can affect atmospheric dynamics [*Markson*, 1981].

Energetic electron precipitation occurring at high latitudes is associated with geomagnetic ULF (1 mHz–1 Hz) waves activity. The ULF waves are observed both in the magnetosphere and on the ground (see *Menk* [2011] for a review) and take energy by the SW through several mechanisms. In the Pc5 frequency range (1–7 mHz) they can be

generated by Kelvin-Helmholtz instability at the SW-magnetosphere boundary or/and by direct penetration into the magnetosphere of waves already present in the interaction regions at the leading edges of the SW high-speed streams [*Regi et al*., 2015]. The Pc5 waves are effective in accelerating to relativistic energies the electrons in the outer radiation belt [*Schulz and Lanzerotti*, 1974], increasing electron flux at geostationary orbit as experimentally observed by GOES measurements [*Baker et al*., 1998; *Rostoker et al*., 1998; *Mathie and Mann*, 2000; *Mann et al*., 2004; *Regi et al*., 2015]. Waves in the Pc1 and Pc2 frequency ranges (100 mHz–1 Hz) are generated near the magnetic equator by unstable distributions of ring current ions during geomagnetic storms. They can induce the electron precipitation process through pitch angle scattering by gyroresonant interaction, as theoretically predicted [*Engebretson et al*., 2008] and experimentally observed [*Rodger et al*., 2008; *Blum et al*., 2015].

Recently, *Francia et al*. [2015] found signatures of ULF geomagnetic activity in the surface air temperature at Terra Nova Bay (TNB, geographical coordinates 74.7°S, 164.1°E); the pulsation power and air temperature appeared significantly correlated, with the air temperature delayed by a few days (3 days for Pc5 and 1 day for Pc1 and Pc2), and supported the electrical mechanism as the possible coupling process between SW-driven geomagnetic perturbations and the low atmosphere conditions. They also found a stronger variability of the temperature during Antarctic winter.

In the present work we compared the SW and interplanetary magnetic field (IMF) parameters and the ULF power P at TNB with the temperature T and the zonal wind speed U fluctuations over Antarctica at different altitudes in the atmosphere. The analysis was performed during 2007, in correspondence to the last declining phase of the solar cycle 23, characterized by recurrent geomagnetic activity associated with SW high-speed streams due to low-latitude coronal holes on the Sun [*Gibson et al*., 2009]. On the basis of *Francia et al*. [2015] observations, we focused particularly on the study of the seasonal dependence.

Our results show a statistically significant relationship between the ULF wave powers and both T and U reanalysis data at altitudes below ~4–5 km (in the troposphere) and above ~8–9 km (in the stratosphere) near to TNB, especially at the 27 day solar synodic rotation period and subharmonics, while around the tropopause ($h \sim 7$–8 km) we do not find any significant relation. Moreover, zonal mean U and T fluctuations at the different altitudes are compared with ULF activity at TNB, and with the polar cap potential difference Φ_{cap}, in the geographical latitude range 60–90°S; the results show that ULF activity is highly related to T and U in the polar region up to ~60°S and in the troposphere ($h < 5$–7 km).

2. Data and Methods

The data of SW velocity (V_{SW}), density (n), and interplanetary magnetic field components (B_x, B_y and B_z), in the geocentric solar ecliptic (GSE) coordinates system, have been provided by OMNIweb (http://cdaweb.gsfc.nasa.gov). The data are sampled at 1 min and are time shifted to the bow shock nose.

We computed the Pc5 (1–7 mHz) and Pc1 and Pc2 (100–500 mHz) geomagnetic horizontal power P by means of Fourier analysis over 1 h nonoverlapped time series of search-coil magnetometer data, recorded at Terra Nova Bay (TNB, corrected geomagnetic coordinates 80.01°S, 306.94°E) at a sampling rate of 1 s; the power spectral densities (PSD) of the H (northward) and D (eastward) components are frequency smoothed, with a final frequency resolution of approximately 1.4 mHz. Since the PSDs of search-coil magnetometer are expressed in $\mathrm{mV}^2/\mathrm{Hz}$, they are converted into $\mathrm{nT}^2/\mathrm{Hz}$ unit using the transfer function of the instrument [*De Lauretis et al*., 2010]. The horizontal PSDs, obtained from the sum of the PSD on the H and D components, are then frequency integrated to obtain the hourly total power P in the Pc5, Pc1 and Pc2 bands, from which we then computed the daily median. Following *Francia et al*. [2015], we used log$P$ instead of P as an activity index of ULF waves, since it is more suitable to be compared with ground temperature variations and follows an almost Gaussian distribution [*Regi et al*., 2015].

As representative parameters of atmospheric conditions, we used the tropospheric and stratospheric temperature T and zonal wind U from ERA-Interim reanalysis data set [see *Simmons et al*., 2007, and references therein], as a function of time t, pressure levels p, geographical latitudes λ, and longitudes φ. ERA-Interim is a global atmospheric reanalysis data set, continuously updated in real time. Global atmospheric and surface parameters from 1 January 1979 to present are available from the surface up to 0.1 hPa as six hourly atmospheric fields on model levels and pressure levels and as three hourly surface fields. The data assimilation system used to produce ERA-Interim is based on a 2006 release of the ECMWF Integrated Forecast Model (IFS Cy31r2). The system

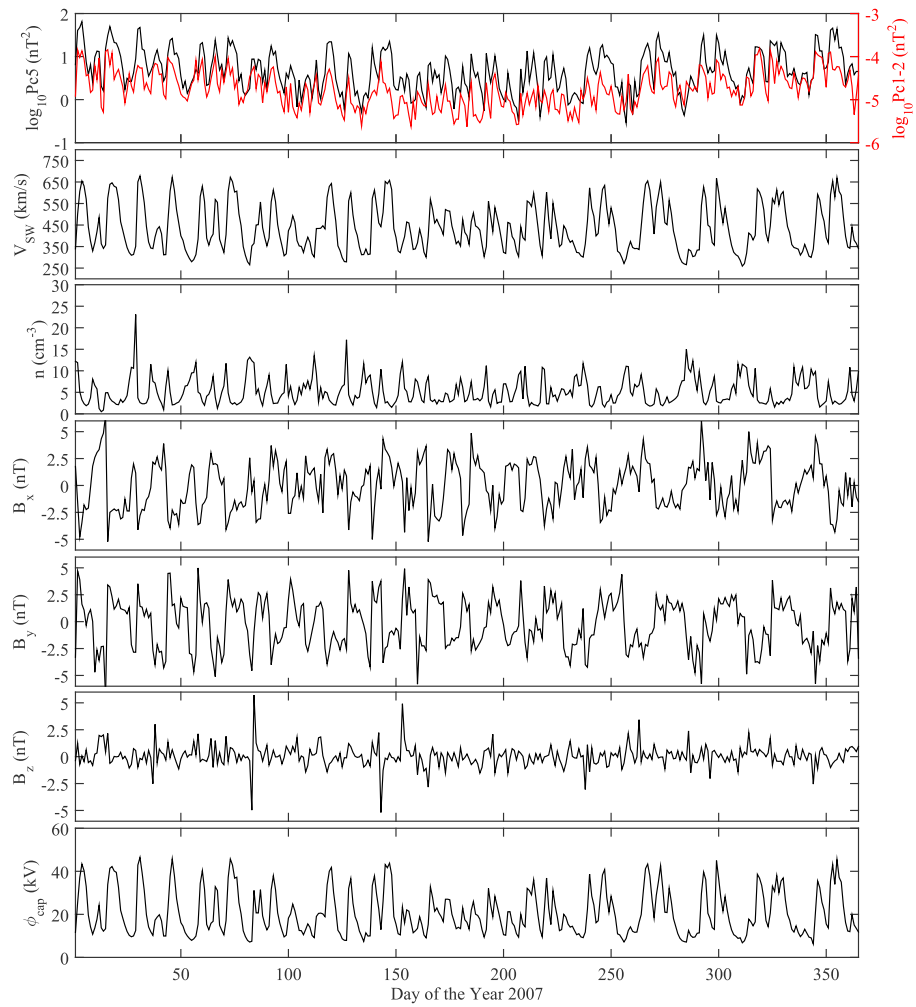

Figure 1. Daily average of the original data sets during 2007; (top to bottom) the ULF activity indexes logPc5, logPc1, and logPc2 at TNB, the solar wind speed V_{SW}, density n, the interplanetary magnetic field components B_x, B_y, and B_z in GSE coordinate system, and the polar cap potential difference ϕ_{cap}.

includes a four-dimensional variational analysis (4D-Var) with a 12 h analysis window. ERA-Interim data used for this study have been retrieved from the Meteorological Archival and Retrieval System at ECMWF.

ERA-Interim data set is useful to study climatic change on the near ground level and up to ~50 km altitude [*Grassi et al.*, 2011; *Seppälä et al.*, 2013]. In our data set the latitude and longitude resolution for T and U are $\Delta\lambda = \Delta\varphi = 2.5°$. Moreover, we used the altitude h instead of p, estimated by the following relation:

$$h(\mathrm{km}) = H ln\left(\frac{p_0}{p}\right) \tag{1}$$

where $H = 7.0$ km, $p_0 = 1000$ hPa and p is expressed in hPa.

In this work we used the SW measurements, the geomagnetic power pulsation, and the reanalysis data set at 1 day time resolution for the whole 2007.

We examined the relationship between T and U data close to TNB, geomagnetic Pc5, Pc1, and Pc2 power, and polar cap potential difference ϕ_{cap} by means of the wavelet coherence and wavelet cross-spectral analysis [*Bendat and Piersol*, 1971; *Grinsted et al.*, 2004]. The continuous wavelet transform is more indicated in non-stationary processes than the Fourier analysis; we used the Morlet wavelet with dimensionless frequency $\omega_0 \approx 6$ to obtain a wavelet scale almost identical to the Fourier periodicity [*Torrence and Compo*, 1998].

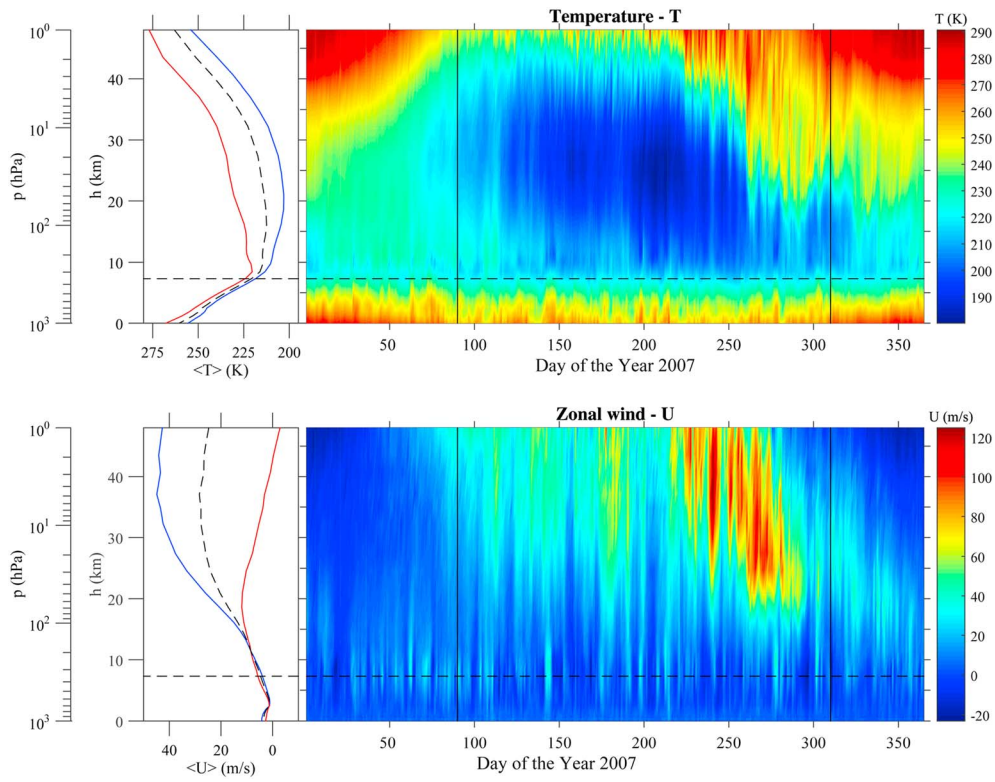

Figure 2. (top) Reanalysis temperature T and (bottom) zonal wind U data from ERA-Interim, as functions of the altitude h above TNB ground station and day of the year 2007 (color scale, right panels); altitude profile of average $< T >$ and $< U >$ over all 2007 (dashed) and during the winter (blue line) and summer (red line) months (left panels); the vertical black dashed lines separate the different seasons. The estimated tropopause position during 2007 is shown with a horizontal dashed line (~7–8 km). The pressure level p is also reported.

The IMF B_z component is particularly important in the energy transfer from SW to the magnetosphere. Indeed, during the coupled ($B_z < 0$) IMF-magnetosphere conditions, it drives the SW electric field $\mathbf{V} \times \mathbf{B}$ into the magnetosphere, influencing the polar cap potential difference ϕ_{cap}. In this work we used the steady state polar cap potential difference ϕ_{cap} following the empirical expression by *Boyle et al*. [1997]:

$$\phi_{\text{cap}} = 1.01 \cdot 10^{-4} V_{\text{SW}}^2 + 11.7 \cdot B \cdot \sin^3 \frac{\theta}{2} \tag{2}$$

where $\theta = \sin^{-1}\left(\frac{B_z}{B}\right)$ is the clock angle and B_z is measured in the GSM coordinate system.

We also analyzed the latitude-height dependencies of T and U fluctuations on the ULF power and ϕ_{cap} fluctuations, assuming TNB power as a proxy for the polar cap ULF power [*Yagova et al*., 2002; *Francia et al*., 2009].

3. The Time Series

Figure 1 shows the ULF power in the Pc5, Pc1, and Pc2 frequency ranges, the SW speed and density, IMF components (in GSE coordinate system), and ϕ_{cap} during 2007. Intense activity in the Pc5, Pc1, and Pc2 bands is observed through the year in correspondence to SW stream occurrence, i.e., in correspondence to high SW speed; in particular, it can be seen a predominant ~13.5 and ~27 day periodicity during the first and last months of 2007, respectively. As matter of fact, *Regi et al*. [2015] observed a strong correlation between the SW structure and the Pc5 pulsation power, with maximum values in correspondence to the corotating interaction regions, ahead of the streams.

Figure 2 shows T and U as a function of time and altitude h; in the left panels their time averaged profiles during winter and summer months are shown versus altitude. In accordance with *Francia et al*. [2015] observations, the T reanalysis data are characterized by a strong variability during the local winter (day of year (DOY) 90–310) at $h \sim 0$–15 km (i.e., in the troposphere and lower stratosphere), while during the summer months

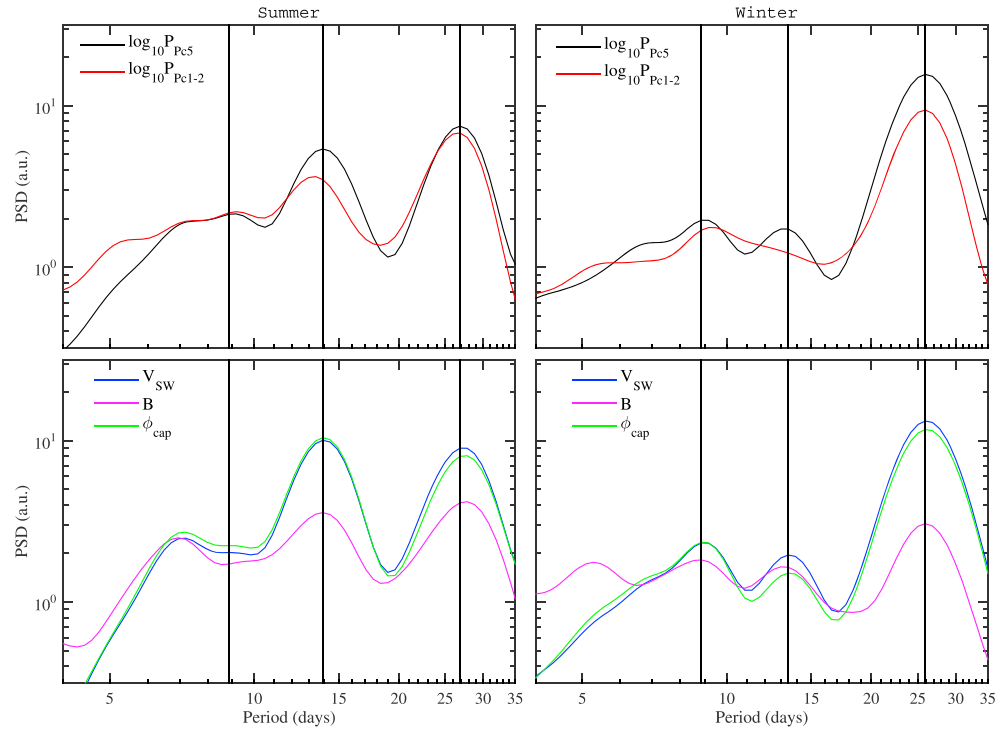

Figure 3. The normalized global wavelet (GW) analysis during the (first column) summer and (second column) winters of 2007, in arbitrary units. (top row) The GW, normalized to the corresponding variances, of the ULF activity indexes logPc5 (black) and logPc1 and logPc2 (red) at TNB; (bottom row) the normalized GW of the solar wind speed V_{SW} (blue), interplanetary magnetic field strength B (magenta) and polar cap potential difference ϕ_{cap} (green). The relative maximum values of the normalized GW of V_{SW} are marked in all corresponding winter and summer related panels with vertical lines.

(DOY 1–89 and 311–365), the T variations are reduced. The zonal wind also shows an increasing fluctuation level during the local winter in the stratosphere, at altitudes well above 10 km. The time-averaged temperature profiles $< T >$ shows the tropopause (the altitude that corresponds to the inversion in the vertical temperature gradient) located approximately between 7 and 10 km, slightly higher during winter. In fact, as expected by the climatology [see, e.g., *Grise et al.*, 2010, and references therein] the tropopause position exhibits a seasonal cycle, and in the southern polar regions the tropopause is lowest in summer (around 7–8 km) and highest in winter (around 10–11 km). The average zonal wind $< U >$ is quite constant up to 10 km and shows a sharp increase starting from ~ 15 km better observed during winter months, with the maximum value at ~40 km.

4. The Frequency/Time Analysis

In the following analysis we prewhitened the data sets by removing the main intrinsic periodicities at ~365 and ~182 days [see *Francia et al.*, 2015], that could otherwise obscure weaker effects.

Figure 3 shows the global wavelet (GW) normalized to the corresponding variance, i.e., the time-averaged wavelet [*Torrence and Compo*, 1998] separately for summer and winter months, of Pc5, Pc1, and Pc2 power at TNB, and V_{SW}, B and ϕ_{cap}. Common power peaks emerge at ~27 days, the synodic Sun rotation period, and its first subharmonics (13.5 and 9 days), in the SW-related parameters and correspondingly in the ULF activity.

5. Cross-Wavelet and Coherence Analysis

In order to investigate the possible correspondence between the parameters, we computed the wavelet coherence γ^2 and cross-wavelet amplitude W_{xy} [*Grinsted et al.*, 2004], considering Pc5, Pc1, and Pc2 indexes, and ϕ_{cap} as inputs and U and T as outputs, for each altitude above TNB ground station. The combined use of both coherence and cross-wavelet allows us a more correct interpretation of the results; indeed, T and U fluctuation power level depends on the season (and therefore the corresponding cross wavelet), while the coherence represents a normalized measure which can reveal common features even though the power is low.

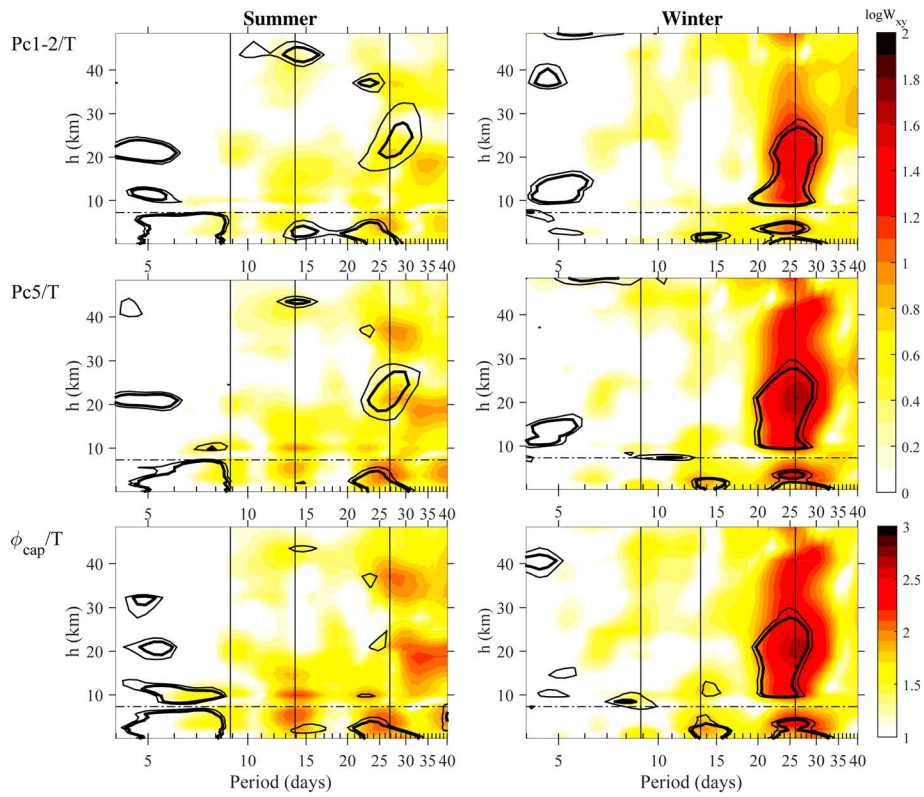

Figure 4. Time averaged cross-wavelet amplitude (color scale) between *T* and geomagnetic ULF activity index (top) logPc1 and logPc2, (middle) logPc5, and (bottom) polar cap potential difference ϕ_{cap} during summer (left) and winter (right) months of 2007 at TNB, as a function of periodicities and altitude *h*. In each panel, the black contour lines mark the 90% (thin) and 95% (bold) significance level of time-averaged wavelet coherence, while the relative maximum values in the GW of V_{SW} (see Figure 3) are marked in all corresponding winter- and summer-related panels with vertical lines, and the horizontal dashed line marks the tropopause position.

In our analysis we computed the time-averaged wavelet coherence $<\gamma^2>$ and cross-wavelet amplitude $<W_{xy}>$ for the different seasons.

For each $<\gamma^2>$ we also estimated the corresponding significance level through Monte Carlo test, computing the time averages over 1000 samples of γ^2, each computed between two independent white noise time series, x_n (inputs) and y_n (outputs), taking into account the actual degree of freedom of each time series. At the examined periodicities and for a given confidence level, the coherence threshold increases with the value of the periodicity [*Grinsted et al.*, 2004]. Moreover, since we whitened the time series before coherence analysis, the autocorrelation at a lag of 1 day is considerably reduced, and hence, the use of white noise (instead of red noise) in the Monte Carlo test is appropriate.

Figure 4 shows, in a color scale, the wavelet cross-spectra amplitude W_{xy} resulting from the Pc5, Pc1, and Pc2 indexes, ϕ_{cap}, (inputs) and *T* (output) during summer and winter months of 2007, and the corresponding 90% and 95% coherence threshold (thin and thick black line contours, respectively). The main periodicities are marked by vertical lines.

The correspondence at 27 days is high and statistically significant in both the troposphere and the stratosphere during winter months, while at 13.5 days it is restricted to $h < 10$ km. During summer W_{xy} attains very low values and a less clear correspondence at the 27 day periodicity for all input parameters. Interestingly, a W_{xy} and γ^2 attenuation can be seen, especially during winter months, near to the tropopause position (~7–10 km). It is worth noting that the highest coherence (not shown in the Figure) is found during winter, at the ~27 day periodicity, for the pair Pc1 and Pc2/*T* in the stratosphere, suggesting that the electron precipitation, related to Pc1 and Pc2 pulsations, plays a major role in the geomagnetic-atmospheric interaction.

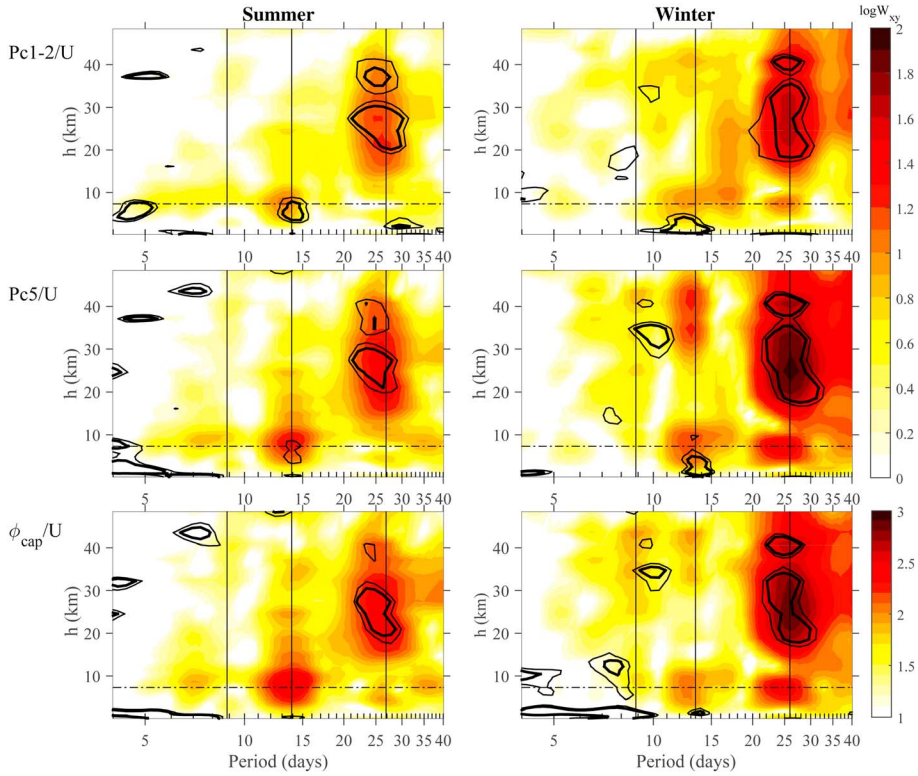

Figure 5. Time averaged cross-wavelet amplitude (color scale) between *U* and geomagnetic ULF activity index (top) logPc1 and logPc2, (middle) logPc5, and (bottom) polar cap potential difference ϕ_{cap} during summer (left) and winter (right) months of 2007 at TNB, as a function of periodicities and altitude *h*. In each panel, the black contour lines mark the 90% (thin) and 95% (bold) significance level of time-averaged wavelet coherence, while the relative maximum values in the GW of V_{SW} (see Figure 3) are marked in all corresponding winter- and summer-related panels with vertical lines, and the horizontal dashed line marks the tropopause position.

Figure 5 shows the W_{xy} calculated using *U* as output parameter. In this case, high and significant W_{xy} and γ^2 values are found mostly in the stratosphere, at ~27 and ~13.5 day periodicities, during winter months. During summer the pattern is similar but with lower values.

6. Latitudinal Dependence

In order to examine the correspondence between geomagnetic and atmospheric parameters over the whole polar cap and at lower latitudes, we computed the zonal mean *T* (i.e., the longitudinal averages of reanalysis data), at different geographical latitudes, and compared it with the previously examined input parameters. We note that Pc5/Pc1 and Pc2 activity indexes are computed at TNB ground station. As a matter of fact, *De Lauretis et al.* [2010] found a significant coherence between geomagnetic field fluctuations at TNB (close to the polar cusp near local magnetic noon, ~20 UT) and Dome C (in the polar cap) during 2005. Assuming that the ULF activity index at TNB can be regarded as a polar cap geomagnetic activity proxy, we computed the coherence analysis with the zonal mean *T*.

Figure 6 shows the time-averaged coherence (color scale) of the zonal *T* with Pc5, Pc1, and Pc2, ϕ_{cap} as a function of geographical latitude and altitude over the Southern Hemisphere during summer and winter months of 2007, for the periodicity of ~27 days. Taking into account the orography in the Southern Hemisphere, we calculated the zonal median position of the land surface (green dashed line).

We found a significant high level of coherence, for all input parameters, from the ground up to ~7–8 km in summer and 10 km in winter (i.e., below the tropopause) for geographic latitudes >70–75°S, i.e., in the polar cap. At these latitudes the coherence increases again above the tropopause. At latitudes <65–60°S the coherence is significantly high only at altitudes >10 km (i.e., in the stratosphere), more evident for the pair Pc1 and Pc2/T, while at $h \sim 0$ km (i.e., at sea level), it attains minimum values.

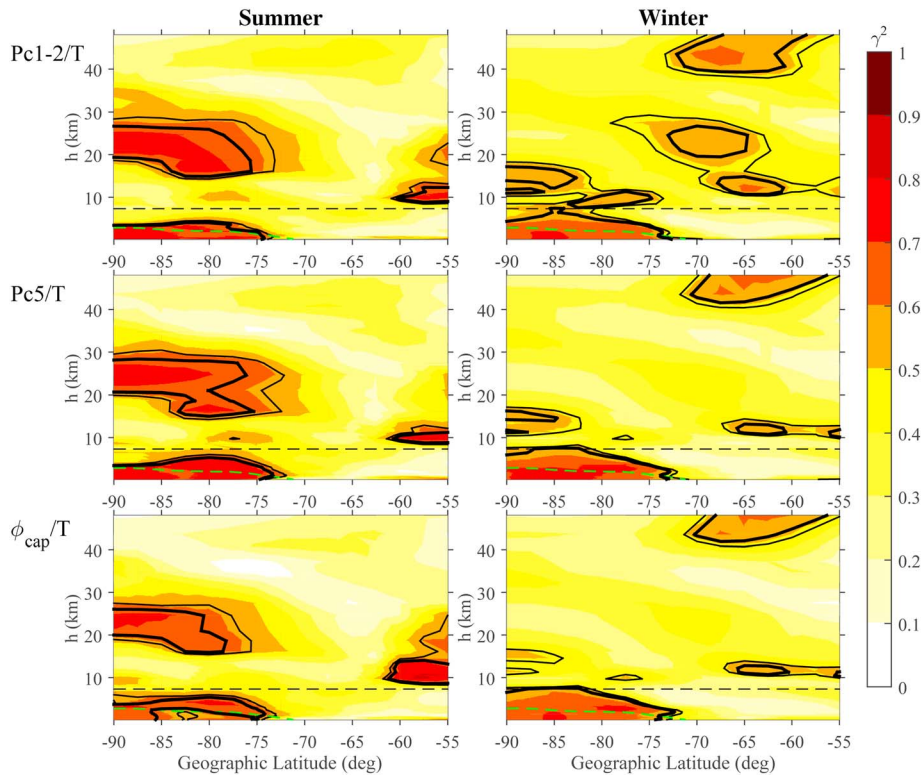

Figure 6. The time-averaged wavelet coherence γ^2 (color scale) at the ~27 days periodicity between the geomagnetic ULF activity index (top) logPc1 and logPc2, (middle) logPc5, and (bottom) polar cap potential difference, with zonal mean *T* during summer (left) and winter (right) months of 2007, as a function of geographical latitude and altitude *h*. In each panel, the zonal median altitudinal profile of the lands are marked with green dashed line; the black contour lines mark the 90% (thin) and 95% (bold) significance level; the horizontal dashed line marks the tropopause position.

In order to further investigate this aspect, we computed in a separate analysis the coherence between logPc5 and *T* at middle latitudes, using geomagnetic data recorded at Macquarie Island ground station (MCQ, geographic coordinates 54.5°S, 158.95°E, corrected geomagnetic latitude 64.28°S). These data are available from International Real-time Magnetic observatory Network (INTERMAGNET) database (http://www.intermagnet.org/) at 1 min sampling period. The coherence shows the same features observed at TNB, with a lower coherence level in the polar cap, probably due to the larger distance of MCQ with respect to TNB.

This result indicates that, at the 27 day periodicity, in the polar cap the tropospheric and stratospheric temperature variations are related to the ULF waves induced in the magnetosphere by SW perturbations (and measured on the ground). At midlatitudes, high coherence is locally observed only in the stratosphere.

7. Summary and Discussion

In the present work we investigated the possible coupling between geomagnetic activity and the low atmosphere dynamics in the southern polar cap during 2007, in correspondence to the last declining phase of the solar cycle 23 which was characterized by recurrent, fast solar wind streams emanating from low-latitude coronal holes on the Sun.

It follows a previous analysis by *Francia et al*. [2015], who found a significant correlation between surface air temperature and ULF power fluctuations at TNB in Antarctica during the winter months in 2007–2008.

Applying the wavelet coherence and cross-wavelet analysis, we compared the polar cap potential difference, derived from the solar wind speed and interplanetary magnetic field, and the ULF geomagnetic pulsations power at TNB with temperature *T* and zonal wind *U* at different heights in the atmosphere over TNB. We examined separately the local summer and winter, which are characterized by different levels of the temperature and zonal wind variability.

The results show that both *T* (Figure 4) and *U* (Figure 5) are related with geomagnetic ULF power and the polar cap potential difference at the periodicities of 27, 13.5, and 9 days, which characterize the solar wind speed and interplanetary magnetic field and the geomagnetic activity in the examined time period. In particular, the correspondence is found in the troposphere at all the periodicities while in the stratosphere it is evident only at 27 days. Moreover, the correspondence strongly reduces around the tropopause position. These results are less clear during the local summer, probably due to the dominant effect of the stable solar radiation on the polar atmosphere.

The significantly high coherence observed between the polar cap potential difference and the temperature and zonal wind makes evident the important role of the solar wind electric field in the atmospheric dynamics. Indeed, its variations during perturbed geomagnetic conditions can affect the cloud layer formation in the troposphere, as suggested by *Tinsley et al*. [2007] and *Troshichev et al*. [2003, 2004, 2008] and *Troshichev and Janzhura* [2004]. Since the polar cap potential variations (related to the interplanetary conditions) modulate the ionosphere-ground potential difference and the associated vertical electric currents (in addition to the increase of conductivity due to the electron precipitation), a ~27 day periodicity in meteorological parameters is expected, in agreement with our observations.

The examined latitude-altitude relationship between ULF activity index and ϕ_{cap} with the zonal mean *T* (Figure 6), at the ~27 days period, reveals that very high coherence is found in the polar cap (i.e., 75–90°S), while it decreases quickly at lower latitudes. It reaches minimum values at latitudes $<$65–70°S, i.e., at latitudes lower than the average equatorward auroral oval border. This result indicates that the ~27 day correlation is a characteristic of the polar cap region both in the troposphere and in the stratosphere.

In conclusion, our investigation shows a significantly high correlation between ULF power fluctuations in the Pc5, Pc1 and Pc2 frequency ranges, and the polar cap potential difference with atmospheric temperature and winds. The ULF inputs are probably responsible for the diffusion/precipitation processes of relativistic electrons from the radiation belts that can modify the atmospheric conductivity, while the input related to the interplanetary electric field probably acts as an additional high-latitude voltage generator in the GEC model (external driver), both altering electric currents in the atmosphere and thereby possibly affecting the occurrence of cloud layer that changes the radiative balance.

Acknowledgments
This research activity was supported by the Italian PNRA (Programma Nazionale di Ricerche in Antartide, PdR2013/B2.09). ERA-Interim reanalysis data were provided by the European Centre for Medium-Range Weather Forecasts (ECMWF). The authors acknowledge J.H. King and N. Papatashvilli at NASA and CDAWeb for solar wind data (http://cdaweb.gsfc.nasa.gov). We thank Geoscience Australia for MCQ ground geomagnetic data and for supporting its operation and INTERMAGNET for promoting high standards of magnetic observatory practice (www.intermagnet.org). Measurements of the magnetic field fluctuations at Terra Nova Bay can be requested from Marcello De Lauretis at the following e-mail address: marcello.delauretis@aquila.infn.it.

References

Andersson, M. E., P. T. Verronen, S. Wang, C. J. Rodger, M. A. Clilverd, and B. R. Carson (2012), Precipitating radiation belt electrons and enhancements of mesospheric hydroxyl during 2004–2009, *J. Geophys. Res.*, *117*, D09304, doi:10.1029/2011JD017246.

Baker, D. N., T. I. Pulkkinen, K. X. Li, and S. G. Kanekal (1998), Coronal mass ejections, magnetic clouds and relativistic magnetospheric electron events: ISTP, *J. Geophys. Res.*, *103*, 17,279–17,291, doi:10.1029/97JA03329.

Baumgaertner, A. J. G., A. Seppälä, P. Joeckel, and M. A. Clilverd (2011), Geomagnetic activity related NOx enhancements and polar surface air temperature variability in a chemistry climate model: Modulation of the NAM index, *Atmos. Chem. Phys.*, *11*(9), 4521–4531, doi:10.5194/acp-11-4521-2011.

Bendat, J., and A. Piersol (1971), *Random Data: Analysis Measurement Procedures*, John Wiley, New York.

Blum, L. W., et al. (2015), Observations of coincident EMIC wave activity and duskside energetic electron precipitation on 18–19 January 2013, *Geophys. Res. Lett.*, *42*, 5727–5735, doi:10.1002/2015GL065245.

Boyle, C. B., P. H. Reiff, and M. R. Hairtson (1997), Empirical polar cap potentials, *J. Geophys. Res.*, *102*(A1), 111–125, doi:10.1029/96JA01742.

De Lauretis, M., P. Francia, M. Regi, U. Villante, and A. Piancatelli (2010), Pc3 pulsations in the polar cap and at low latitude, *J. Geophys. Res.*, *115*, A11223, doi:10.1029/2010JA015967.

Dudok de Wit, T., and J. Watermann (2010), Solar forcing of the terrestrial atmosphere, *C. R. Geosci.*, *342*, 259–272.

Engebretson, M. J., et al. (2008), Pc1–2 waves and energetic particle precipitation during and after magnetic storms: Superposed epoch analysis and case studies, *J. Geophys. Res.*, *113*, A01211, doi:10.1029/2007JA012362.

Francia, P., M. De Lauretis, M. Vellante, U. Villante, and A. Piancatelli (2009), ULF geomagnetic pulsations at different latitudes in Antarctica, *Ann. Geophys.*, *27*, 1–9.

Francia, P., M. Regi, and M. De Lauretis (2015), Signatures of the ULF geomagnetic activity in the surface air temperature in Antarctica, *J. Geophys. Res. Space Physics*, *120*, doi:10.1002/2015JA021011.

Gibson, S. E., J. U. Kozyra, G. de Toma, B. A. Emery, T. Onsager, and B. J. Thompson (2009), If the Sun is so quiet, why is the Earth ringing? A comparison of two solar minimum intervals, *J. Geophys. Res.*, *114*, A09105, doi:10.1029/2009JA014342.

Grassi, B., G. Redaelli, P. O. Canziani, and G. Visconti (2011), Effects of the PDO phase on the tropical belt width, *J. Clim.*, *25*, 3282–3290.

Gray, L., et al. (2010), Solar influences on climate, *Rev. Geophys.*, *48*, RG4001, doi:10.1029/2009RG000282.

Grinsted, A., J. C. Moore, and S. Jevrejeva (2004), Application of the cross wavelet transform and wavelet coherence to geophysical time series, *Nonlinear Processes Geophys.*, *11*, 561–566.

Grise, K., D. Thompson, and T. Birner (2010), A global survey of static stability in the stratosphere and upper troposphere, *J. Clim.*, *23*(9), 2275–2292, doi:10.1175/2009jcli3369.1.

Lam, M., and B. Tinsley (2015), Solar wind-atmospheric electricity-cloud microphysics connections to weather and climate, *J. Atmos. Sol.-Terr. Phys.*, doi:10.1016/j.jastp.2015.10.019.

Lockwood, M., R. G. Harrison, T. Woollings, and S. K. Solanki (2010), Are cold winters in Europe associated with low solar activity?, *Environ. Res. Lett.*, *5*(2), 024001, doi:10.1088/1748-9326/5/2/024001.

Lu, H., M. A. Clilverd, A. Seppala, and L. L. Hood (2008), Geomagnetic perturbations on stratospheric circulation in late winter and spring, *J. Geophys. Res.*, *113*, D16106, doi:10.1029/2007JD008915.

Mann, I. R., T. P. O'Brien, and D. K. Milling (2004), Correlations between ULF wave power, solar wind speed, and relativistic electron flux in the magnetosphere: Solar cycle dependence, *J. Atmos. Sol.-Terr. Phys.*, *66*, 187–198, doi:10.1016/j.jastp.2003.10.002.

Markson, R. (1981), Modulation of the Earth's electric field by cosmic radiation, *Nature*, *291*, 304–308.

Mathie, R. A., and I. R. Mann (2000), A correlation between extended intervals of ULF wave power and storm-time geosynchronous relativistic electron flux enhancements, *Geophys. Res. Lett.*, *27*, 3261–3264, doi:10.1029/2000GL003822.

Menk, F. W. (2011), Magnetospheric ULF waves: A review, in *The Dynamic Magnetosphere*, *IAGA Spec. Sopron Book Ser.*, vol. 3, edited by W. Liu and M. Fujimoto, pp. 223–256, Springer, Berlin.

Mironova, I., K. Aplin, F. Arnold, G. Bazilevskaya, R. Harrison, A. Krivolutsky, K. Nicoll, E. Rozanov, E. Turunen, and I. Usoskin (2015), Energetic particle influence on the Earth's atmosphere, *Space Sci. Rev.*, *194*(1–4), 1–96, doi:10.1007/s11214-015-0185-4.

Randall, C. E., et al. (2005), Stratospheric effects of energetic particle precipitation in 2003–2004, *Geophys. Res. Lett.*, *32*, L05802, doi:10.1029/2004GL022003.

Randall, C. E., V. L. Harvey, C. S. Singleton, S. M. Bailey, P. F. Bernath, M. Codrescu, H. Nakajima, and J. M. Russell III (2007), Energetic particle precipitation effects on the Southern Hemisphere stratosphere in 1992–2005, *J. Geophys. Res.*, *112*, D08308, doi:10.1029/2006JD007696.

Regi, M., M. De Lauretis, and P. Francia (2015), Pc5 geomagnetic fluctuations in response to solar wind excitation and their relationship with relativistic electron fluxes in the outer radiation belt, *Earth Planets Space*, *67*, 9, doi:10.1186/s40623-015-0180-8.

Rodger, C. J., T. Raita, M. A. Clilverd, A. Seppala, S. Dietrich, N. R. Thomson, and T. Ulich (2008), Observations of relativistic electron precipitation from the radiation belts driven by EMIC waves, *Geophys. Res. Lett.*, *35*, L16106, doi:10.1029/2008GL034804.

Rostoker, G., S. Skone, and D. N. Baker (1998), On the origin of relativistic electrons in the magnetosphere associated with some geomagnetic storms, *Geophys. Res. Lett.*, *25*, 3701–3704.

Rozanov, E., L. Callis, M. Schlesinger, F. Yang, N. Andronova, and V. Zubov (2005), Atmospheric response to NO y source due to energetic electron precipitation, *Geophys. Res. Lett.*, *32*, L14811, doi:10.1029/2005GL023041.

Rycroft, M., K. Nicoll, K. Aplin, and R. Giles Harrison (2012), Recent advances in global electric circuit coupling between the space environment and the troposphere, *J. Atmos. Sol.-Terr. Phys.*, *90–91*, 198–211, doi:10.1016/j.jastp.2012.03.015.

Schulz, M., and L. J. Lanzerotti (1974), *Physics and Chemistry in Space*, Springer, Berlin.

Seppälä, A., P. T. Verronen, M. A. Clilverd, C. E. Randall, J. Tamminen, V. Sofieva, L. Backman, and E. Kyrölä (2007), Arctic and Antarctic polar winter NOx and energetic particle precipitation in 2002–2006, *Geophys. Res. Lett.*, *34*, L12810, doi:10.1029/2007GL029733.

Seppälä, A., C. E. Randall, M. A. Clilverd, E. Rozanov, and C. J. Rodger (2009), Geomagnetic activity and polar surface air temperature variability, *J. Geophys. Res.*, *114*, A10312, doi:10.1029/2008JA014029.

Seppälä, A., H. Lu, M. A. Clilverd, and C. J. Rodger (2013), Geomagnetic activity signatures in wintertime stratosphere wind, temperature, and wave response, *J. Geophys. Res. Atmos.*, *118*, 2169–2183, doi:10.1002/jgrd.50236.

Seppälä, A., K. Matthes, C. Randall, and I. Mironova (2014), What is the solar influence on climate? Overview of activities during CAWSES-II, *Prog. Earth Planet. Sci.*, *1*(1), 24, doi:10.1186/s40645-014-0024-3.

Simmons, A., S. Uppala, D. Dee, and S. Kobayashi (2007), *ERA-Interim: New ECMWF Reanalysis Products From 1989 Onwards*, *ECMWF Newsl.*, vol. 110, pp. 25–35 , ECMWF, Reading, U. K.

Tinsley, B. (2008), The global atmospheric electric circuit and its effects on cloud microphysics, *Rep. Prog. Phys.*, *71*(6), 066801, doi:10.1088/0034-4885/71/6/066801.

Tinsley, B. A., and L. Zhou (2006), Initial results of a global circuit model with stratospheric and tropospheric aerosols, *J. Geophys. Res.*, *111*, D16205, doi:10.1029/2005JD006988.

Tinsley, B. A., G. B. Burns, and L. Zhou (2007), The role of the global electric circuit in solar and internal forcing of clouds and climate, *Adv. Space Res.*, *40*, 1126–1139, doi:10.1016/j.asr.2007.01.071.

Torrence, C., and G. P. Compo (1998), A practical guide to wavelet analysis, *Bull. Am. Meteorol. Soc.*, *79*, 61–78.

Troshichev, O. A., and A. Janzhura (2004), Temperature alterations on the Antarctic ice sheet initiated by the disturbed solar wind, *J. Atmos. Sol.-Terr. Phys.*, *66*, 1159–1172, doi:10.1016/j.jastp.2004.05.005.

Troshichev, O. A., L. V. Egorova, and V. Y. Vovk (2003), Evidence for influence of the solar wind variations on atmospheric temperature in the southern polar region, *J. Atmos. Sol.-Terr. Phys.*, *65*, 947–956, doi:10.1016/S1364-6826(03)00112-3.

Troshichev, O. A., L. V. Egorova, and V. Y. Vovk (2004), Influence of the solar wind variations on atmospheric parameters in the southern polar region, *Adv. Space Res.*, *43*, 1824–1829, doi:10.1016/j.asr.2003.06.034.

Troshichev, O., V. Vovk, and L. Egorova (2008), IMF-associated cloudiness above near-pole station Vostok: Impact on wind regime in winter Antarctica, *J. Atmos. Sol.-Terr. Phys.*, *70*, 1289–1300, doi:10.1016/j.jastp.2008.04.003.

Verronen, P. T., M. L. Santee, G. L. Manney, R. Lehmann, S.-M. Salmi, and A. Seppälä (2011), Nitric acid enhancements in the mesosphere during the January 2005 and December 2006 solar proton events, *J. Geophys. Res.*, *116*, D17301, doi:10.1029/2011JD016075.

Yagova, N., L. Lanzerotti, U. Villante, V. Pilipenko, S. Lepidi, P. Francia, V. Papitashvili, and A. Rodger (2002), ULF Pc5-6 magnetic activity in the polar cap as observed along a geomagnetic meridian in Antarctica, *J. Geophys. Res.*, *107*(A8), 1195, doi:10.1029/2001JA900143.